FULL PAPER

Dalton
www.rsc.org/dalton

$Cu(HCO_2)_2L$ {L = pyrazine, 4,4′-bipyridine}: employing the formate anion as a building block in three-dimensional coordination polymers †

Jamie L. Manson,*[a,b] Jana G. Lecher,[a] Jiyeong Gu,[a] Urs Geiser,[a] John A. Schlueter,[a] Robert Henning,*‡[c] Xiaoping Wang,[c] Arthur J. Schultz,[c] Hyun-Joo Koo[d] and Myung-Hwan Whangbo[d]

[a] *Materials Science Division, Argonne National Laboratory, Argonne, IL 60439-4831, USA*
[b] *Condensed Matter Sciences Division, Oak Ridge National Laboratory, Oak Ridge, TN 37831-6430, USA*
[c] *Intense Pulsed Neutron Source, Argonne National Laboratory, Argonne, IL 60439-4831, USA*
[d] *Department of Chemistry, North Carolina State University, Raleigh, NC 27695-8204, USA*

Received 7th March 2003, Accepted 29th May 2003
First published as an Advance Article on the web 18th June 2003

The formate anion, HCO_2^-, has been used infrequently as a building block in molecular magnetic materials. We have synthesized and structurally and magnetically characterized two new $Cu(HCO_2)_2L$ compounds, where L represents pyrazine (pyz) and 4,4′-bipyridine (bipy). The single crystal structure of $Cu(HCO_2)_2$(pyz), **1**, has been established by both X-ray (295 K) and neutron diffraction (20 K). The compound consists of tetragonally-elongated CuN_2O_4 octahedra made up of four bridging formate anions and two neutral pyz ligands. The 3D polymeric network is comprised of 2D $Cu(HCO_2)_2$ layers that are fused together by the linear pyz spacers, which form Cu–pyz-Cu chains. $Cu(HCO_2)_2$(bipy), **2**, is chiral and has a more complex framework than **1**. The CuO_4N_2 octahedra align in two unique orientations relative to one another, owing to the 4_1 and 2_1 screw axes that lie along the *a* and *b*-axes. The octahedra are connected *via* four bridging HCO_2^- anions and two bridging bipy ligands, resulting in a unique 3D scaffold structure. The magnetic behavior of **1** and **2** indicates antiferro- and ferromagnetic interactions, respectively, and the exchange couplings in both **1** and **2** are well reproduced by a 1D spin Hamiltonian. Spin dimer analysis was carried out to evaluate the relative strengths of the various spin exchange paths. It is found that the interaction through HCO_2^- is comparatively weak, and the strong Cu^{2+} spin exchange interactions are mediated by the pyz and bipy ligands *via* the σ-pathway. A possible reason as to why **2** displays ferromagnetic coupling is proposed.

1 Introduction

A rich variety of coordination polymers with interesting magnetic behavior have been obtained by combining paramagnetic transition metal ions and small molecular subunits such as CN^-,[1] N_3^-,[2] ox^{2-} (ox = oxalate),[3] and many others. Strikingly, the formate anion, HCO_2^-, which is also the simplest carboxylate, has been used very infrequently as a building block, although acetate, $CH_3CO_2^-$, and several others have been.[4] While each of these anions possesses potentially *bis*-coordinating oxygen atoms, $CH_3CO_2^-$ tends to favor formation of transition metal-dimer motifs, *i.e.* $M_2(CH_3CO_2)_4$·solvent, which hampers the construction of multidimensional magnetic solids. Moreover, the unpaired electrons are typically restricted to the dimeric unit, affording very strong intramolecular antiferromagnetic coupling.[5]

Simple metal–formate hydrates have long been known.[6] $Cu(HCO_2)_2(H_2O)_2$·$2H_2O$ has received the most research interest, even very recently, owing to its quantum spin state and relationship to high-T_c cuprate superconductors.[7] The crystal structures of these simple salts consist of two-dimensional polymeric networks that involve bridging μ-HCO_2^- formate anions and hydrogen bonding between coordinated and non-coordinated water molecules.[8] Antiferromagnetic exchange interactions, which are mediated by the formate ligand, lead to pronounced 2D magnetic behavior while weaker interlayer interaction *via* H_2O molecules affords a Néel temperature of 17 K.[6a] Quantum-spin magnetic systems, especially confined to one- or two-dimensions, have been an active area of investigation for many years. Thus, systems such as copper(II) formate tetrahydrate, $Cu(HCO_2)_2(H_2O)_2$·$2H_2O$, are particularly attractive and have been studied with a number of physical tools so that a fundamental understanding of the correlation between lattice and spin dimensionality may be gained. The purpose of the current work was to modify the structure of the parent $Cu(HCO_2)_2(H_2O)_2$·$2H_2O$ by replacing the H_2O molecules with bridging organic ligands in an effort to assemble 3D networks, as well as to systematically modulate the magnetic exchange coupling.

In this paper, we report the successful chemical modification, crystal structures, magnetic behavior and electronic structure calculations for two new Cu^{2+} formate derivatives, $Cu(HCO_2)_2$(pyz) {pyz = pyrazine}, **1**, and $Cu(HCO_2)_2$(bipy) {bipy = 4,4′-bipyridine}, **2**. The two compounds demonstrate strong 1D magnetic exchange, which is propogated *via* the pyz and bipy bridging ligands.

2 Experimental

2.1 Synthesis

$Cu(HCO_2)_2$(pyz), 1. To a vigorously stirring 10 mL aqueous solution of $Cu(HCO_2)_2$·yH_2O (3.26 mmol, 0.500 g) was added a 5 mL ethanolic solution containing pyz (7.5 mmol, 0.600 g). A blue solid precipitated immediately from solution that was allowed to stir an additional 1 h at room temperature. The blue microcrystalline solid was collected by suction filtration and dried *in vacuo* for ~8 h, yielding 0.454 g of **1** (60% yield). The additional product in the form of large single crystals may be obtained by allowing the filtrate solution to stand undisturbed at room temperature for ~3 months. The powder and single

† Electronic supplementary information (ESI) available: Table S1, Exponents and valence shell ionization potentials. See http://www.rsc.org/suppdata/dt/b3/b302631k/

‡ Permanent address: Advanced Photon Source, Argonne National Laboratory, Argonne, IL 60439-4831.

DOI: 10.1039/b302631k

crystal samples were determined to be identical as shown by IR spectroscopy and a comparison between calculated and observed X-ray powder diffraction patterns.

$Cu(HCO_2)_2(bipy)$, 2. To a 10 mL aqueous solution containing $NaHCO_2$ (0.75 mmol, 0.051 g) and $Cu(HCO_2)_2 \cdot yH_2O$ (1.50 mmol, 0.339 g) was added a 5 mL acetone solution of 4,4′-bipy (3.00 mmol, 0.469 g). While stirring, a blue precipitate formed quickly which was allowed to stir an additional 1 h at room temperature. The obtained blue powder was collected by suction filtration and dried *in vacuo* for ~5 h, yielding 0.390 g of **2** (84% yield). Single crystals of **2** in the form of deep blue cubes were obtained by slow solvent evaporation of the filtrate over a 2 week period. From IR spectroscopy and comparative analysis of X-ray powder diffraction data, we concluded that both the powder and single crystal samples of **2** were of identical composition.

2.2 Single crystal structure determinations

X-ray diffraction. For **1** and **2**, respectively, blue blocks measuring 0.3 × 0.2 × 0.2 and 0.15 × 0.15 × 0.15 mm were adhered to glass fibers and mounted on a Bruker AXS X-ray diffractometer equipped with a SMART CCD area detector. Monochromated MoKα radiation (λ = 0.71073 Å) was used in the data collection. Approximately a hemisphere of data was measured to a resolution of 0.75 Å at room temperature. The area detector frames were integrated by use of the program SMART, and the resulting intensities absorption corrected by gaussian integration (SHELXTL program suite). The SHELXTL program package was employed in the structure solution using direct methods, full matrix least-squares refinement on F^2 (using all data) and some graphics. Positions of aromatic H atoms were calculated by employing a 'riding' model with an isotropic displacement parameter 20% larger than the equivalent isotropic displacement parameter of the atom to which the H atom is attached. No correction for extinction was required.

Neutron diffraction. Neutron diffraction data were collected on a large single crystal of $Cu(HCO_2)_2(pyz)$, **1**, at the Intense Pulsed Neutron Source (IPNS), Argonne National Laboratory. The single-crystal diffractometer, SCD, is a time-of-flight (TOF) instrument with time- and position-sensitive detectors. Neutrons are produced by the pulsed (30 Hz) spallation source at IPNS, and the SCD instrument uses the entire thermal spectrum of neutrons from each pulse. The SCD position-sensitive neutron detector contains a ^{6}Li-glass scintillator with dimensions of 30 × 30 cm^2. For a given crystal setting, data are stored in a three-dimensional histogram in which each point has coordinates x, y, and t, which are the horizontal and vertical detector positions and the TOF, respectively. t is related to the neutron wavelength λ by the de Broglie equation $\lambda = (h/m)(t/l)$, in which h is Planck's constant, m is the neutron mass, and l is the path length traversed in time t. There are 120 time-of-flight channels in each histogram, constructed in such a way that $\Delta t/t$ has a constant value of 0.015. Each histogram comprises measurements of a three-dimensional block of reciprocal space, from neutrons in the wavelength range of 0.71–4.2 Å. A detailed description of the SCD instrument and data collection and analysis procedures has been given in the literature.[9,10] The sample temperature was controlled using an Air Products and Chemicals, Inc. model CS-202 closed-cycle helium refrigerator.

The initial orientation matrix was obtained using an autoindexing algorithm[11] of peaks in a single histogram. The occurrence of the *C*-centered phase at the temperature of the experiment was verified. For intensity data collection, 17 histograms were measured, each for a different crystal setting, in order to cover a unique quartet of reciprocal space. Bragg peaks were integrated in three dimensions about their predicted locations and were corrected for the incident neutron spectrum, detector efficiency, and deadtime loss. Lorentz and absorption corrections were also applied. The structure was refined with the program SHELXL97.[12] In the final least-squares cycle, all atoms including hydrogen were refined with anisotropic temperature factors. A summary of parameters related to the neutron diffraction experiment is presented in Table 1. Selected bond distances and angles of **1** and **2** are listed in Tables 2 and 3, respectively.

CCDC reference numbers 205743, 204744 and 211672.

See http://www.rsc.org/suppdata/dt/b3/b302631k/ for crystallographic data in CIF or other electronic format.

2.3 Magnetic measurements

Low temperature ac susceptibility measurements (T < 4.5 K) were performed on a Lakeshore model ACS 7000 susceptometer equipped with a 5 T superconducting magnet. Powder samples weighing ~50–100 mg were loaded in Delrin holders and mounted to the end of the sample rod. Measurements entailed cooing of the sample in zero-field to the lowest desired temperature, generally 1.6 K, and data collected upon warming. A 1 Oe drive field oscillating at 125 Hz was employed during the measurements. Dc magnetization data were limited to T > 4.5 K and collected using a Quantum Design MPMS-7 SQUID magnetometer. Smaller samples, typically weighing 30–50 mg, were loaded into gelatin capsules, mounted in a plastic straw and attached to the end of the sample rod. A 6 cm scan length was used as it provided sufficient sensitivity for these measurements. The samples were zero-field cooled to 4.5 K, the dc field charged to 1 kOe, and data taken upon warming to 300 K. Plots of χT shown here were made by merging our low-T ac and higher-T magnetic susceptibility data. Field-dependent $M(H)$ experiments up to 7 T were made at 4.5 K using the SQUID. All magnetic data were corrected for core diamagnetism that was -162×10^{-6} and -221×10^{-6} emu mol^{-1} for **1** and **2**, respectively, as determined from Pascal's constants.

3 Crystal structures of $Cu(HCO_2)_2(pyz)$, 1, and $Cu(HCO_2)_2(bipy)$, 2

The present X-ray and neutron diffraction studies show that compound **1** crystallizes in the monoclinic space group *C*2/*c* at 295 and 20 K. The neutron diffraction measurement was made to search for any possible structural phase transitions between the two temperature extremes but none were detected. The difference between the unit cell volumes at 20 and 295 K is ~5% which is attributed to the usual lattice contraction upon cooling and the β-angle decreases from 92.78(2) to 90.235(2)°. An ORTEP diagram showing the Cu^{2+} coordination sphere and the atom-labeling scheme are given in Fig. 1. The CuO_4N_2 chromophore is Jahn–Teller distorted along the $a + b$ direction, with two short Cu–O(1), two long Cu–O(2) and two intermediate

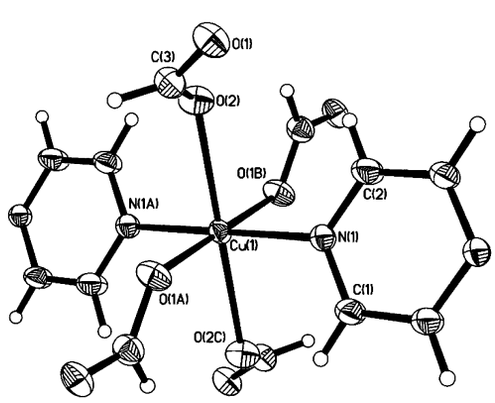

Fig. 1 ORTEP diagram and atom labeling scheme for $Cu(HCO_2)_2(pyz)$, **1**.

Table 1 Crystallographic data for $Cu(HCO_2)_2(pyz)$, **1**, and $Cu(HCO_2)_2(bipy)$, **2**

Compound	$Cu(HCO_2)_2(pyz)$, **1**	$Cu(HCO_2)_2(pyz)$, **1**	$Cu(HCO_2)_2(bipy)$, **2**
Radiation type	X-Ray	Neutron	X-Ray
Formula	$CuC_6O_4N_2H_6$	$CuC_6O_4N_2H_6$	$CuC_{12}O_4N_2H_{10}$
Formula weight	233.67	233.67	309.76
Space group	*C*2/*c*	*C*2/*c*	$P4_12_12$
a/Å	11.5799(11)	11.405(3)	7.8534(2)
b/Å	7.6759(7)	7.510(1)	7.8534(2)
c/Å	8.5592(8)	8.435(2)	18.4799(8)
β/°	90.235(5)	92.78(2)	90
V/Å^3	760.8(1)	721.6(3)	1139.8(1)
Z	4	4	4
T/K	295	20	295
λ/Å	0.71073	TOF, 0.71–4.2	0.71073
μ/mm^{-1}	2.851	1.135 + 0.661*λ*	1.93
$R(F)^a$	0.0312	0.067	0.0228
$R_w(F)^b$	0.0921	0.164	0.0631
GOF	1.180	1.003	1.084

^{a} $R = \Sigma[|F_o| - |F_c|]/\Sigma|F_o|$. ^{b} $R_w = [\Sigma w[|F_o| - |F_c|]^2/\Sigma w[|F_o|^2]]^{1/2}$.

Table 2 Selected bond distances (Å) and bond angles (°) for $Cu(HCO_2)_2(pyz)$, **1**

	X-Ray (298 K)	Neutron (20 K)
Cu–O(1)	1.954(2)	1.940(3)
Cu–O(2)	2.371(2)	2.314(2)
Cu–N(1)	2.083(2)	2.039(2)
C(1)–N(1)	1.336(4)	1.327(3)
C(2)–N(1)	1.333(4)	1.325(2)
C(1)–C(2)	1.385(4)	1.377(3)
C(3)–O(1)	1.258(4)	1.257(3)
C(3)–O(2)	1.233(4)	1.230(4)
O(1)–Cu–O(2)	88.85(9)	89.02(10)
O(1)–Cu–O(1)	180	180
O(1)–Cu–N(1)	89.19(11)	88.88(10)
O(2)–Cu–N(1)	88.85(9)	88.66(7)
Cu–O(1)–C(3)	128.6(2)	127.9(2)
O(1)–C(3)–O(2)	125.2(3)	124.2(2)

Table 3 Selected bond distances (Å) and bond angles (°) for $Cu(HCO_2)_2(bipy)$, **2**

Cu–O(1)	1.977(1)	O(1)–Cu–O(1)	176.70(9)
Cu–O(2)	2.528(2)	O(1)–Cu–O(2)	85.13(7)
Cu–N(1)	2.031(2)	O(1)–Cu–N(1)	88.35(5)
Cu–N(2)	2.015(2)	O(1)–Cu–N(2)	91.65(5)
O(1)–C(7)	1.243(3)	N(1)–Cu–N(2)	180
C(1)–N(1)	1.337(2)	Cu–O(1)–C(7)	129.7(2)

Cu–N(1) bond lengths of 1.954 (2), 2.371 (2) and 2.083 (2) Å (X-ray diffraction) and 1.940 (3), 2.314 (2) and 2.039 (2) Å (neutron diffraction), respectively. As shown by both X-ray and neutron diffraction, the bond angles within the Cu^{2+} octahedron, namely O(1)–Cu–O(2), O(1)–Cu–N(1) and O(2)–Cu–N(1), deviate slightly from 90° and range from 88.9 (1) to 91.1 (1)° and, as required by symmetry, O(1)–Cu–O(1A), O(2)–Cu–O(2A) and N(1)–Cu–N(1A) are 180°. Weak hydrogen bonding between H(3A) and O(2) [2.315 (9) Å] may act to further stabilize the structure. The bond distances and angles within the HCO_2^- and pyz moieties are typical for these species.[8,13] The four equatorial formate anions and two axially-coordinated pyz ligands form bridges to six other CuO_4N_2 octahedra, affording a 3D framework structure, Fig. 2 and 3. Infinite 2D square $Cu(HCO_2)_2$ layers reside in the *bc*-plane that adopt a similar structural arrangement to that observed in $Cu(HCO_2)_2(H_2O)_2{\cdot}2H_2O$. The pyz spacer ligands bridge the layers together with Cu ··· Cu distances of 6.946 Å. The closest Cu ··· Cu separation *via* HCO_2^- is 5.748 Å. A similar 2D-layered structure has recently been reported for $Co(HCO_2)_2(HCONH_2)_2$, where hydrogen bonds between

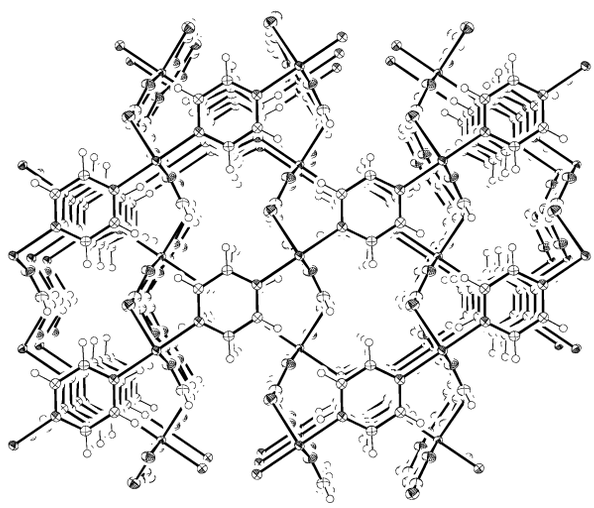

Fig. 2 Perspective view of the crystal structure of **1** viewed normal to the pyz rings.

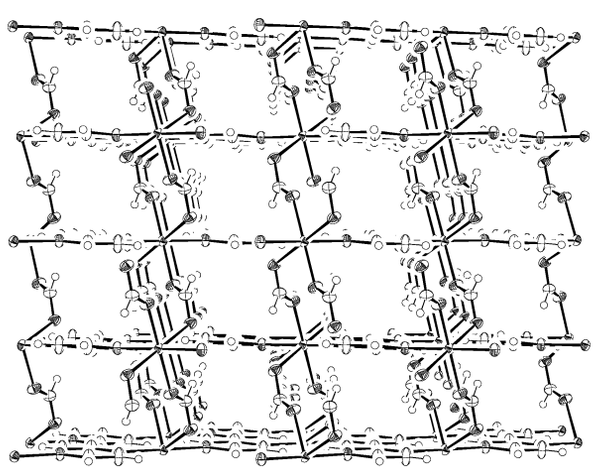

Fig. 3 Alternative view of the scaffold structure of **1** viewed parallel to the (010) direction.

$HCONH_2$ molecules and HCO_2^- fuse the sheets together to yield a weakly held 3D structure.[14]

The single crystal X-ray structure of **2** was determined at room temperature. It crystallizes in the tetragonal space group $P4_12_12$ with $a = 7.8534$ (2), $c = 18.4799$ (8) Å and $V = 1139.75$ (13) Å^3. The Cu^{2+} cation resides at the center of a 4 + 2 tetragonally-elongated octahedron, with Cu–O(1), Cu–O(2), Cu–N(1) and Cu–N(2) bond distances of 1.977 (1), 2.528 (2), 2.031

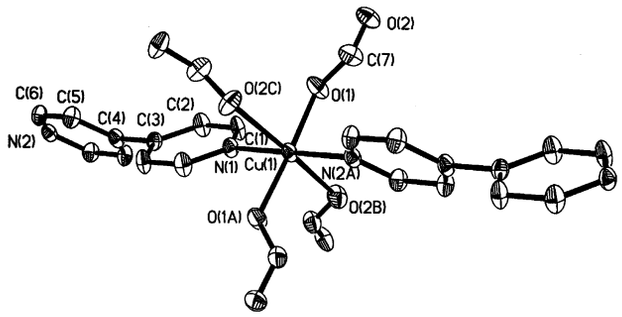

Fig. 4 ORTEP diagram and atom labeling scheme for $Cu(HCO_2)_2$-(bipy), **2**. Hydrogen atoms have been omitted for clarity.

(2) and 2.015 (2) Å, respectively, Fig. 4. Bond angles within the coordination sphere deviate appreciably from the expected 90° angles which range from 85.13 (7) to 94.70 (7)°. The N(1)–Cu–N(2) bond angle is 180° while O(1A)–Cu–O(1) and O(2A)–Cu–O(2) are, respectively, 176.70 (9) and 173.91 (8)°. The sp^2-hybridized oxygen atoms, O(1) and O(2), of the coordinated formate anions make Cu–O(1)–C(7) and Cu–O(2)–C(7) bond angles of 129.7 (2) and 117.2 (2)°, respectively. The aryl rings of the bipy ligand are not coplanar and are twisted relative to one another by 50.5 (2)°. All other bond distances and angles of the HCO2- and bipy ligands agree with those observed in other systems.[2a,2i,8,13] The extended structure is a 3D coordination polymer but it differs from that of **1**, Fig. 5. For **2**, each HCO_2^- anion and 4,4′-bipy bridge two Cu^{2+} centers and thus each CuO_4N_2 octahedron is vertex connected to six other octahedra. Neighboring 1D linear Cu–bipy-Cu chains are alternately rotated by 90° and propogate parallel to the (110) and (−110) directions. In contrast to **1** and the parent $Cu(HCO_2)_2(H_2O)_2 \cdot 2H_2O$ compound, the square layers are not retained: see Fig. 6, which shows only the formate connectivity of the Cu cations within **2**. Note the edge-sharing *chair*-cyclohexane type conformation adopted by the Cu ions and the relationship to the diamond lattice. As a result, a chiral 3D framework is formed which is reminiscent to the Mn–azide complex, $Mn(N_3)_2$-(bipy).[2i] The shortest metal–metal separation is 6.067 Å *via* Cu–OC(H)O–Cu bonds, which is 0.319 Å (5.4%) longer than those in **1**.

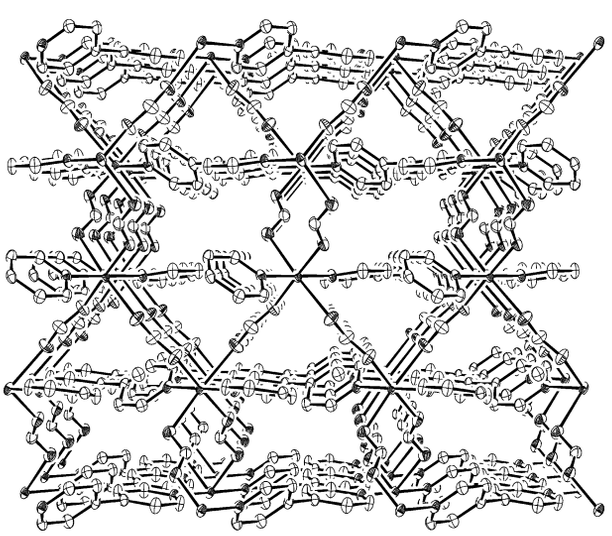

Fig. 5 Crystal structure of **2** viewed along the (100) direction. Hydrogen atoms have been omitted for clarity.

The four short bonds of each CuO_4N_2 octahedron (*i.e.*, two Cu–O and two Cu–N bonds) in **1** and **2** forms a CuO_2N_2 "square". The CuO_2N_2 "squares" are arranged in a 3D pattern such that the N–Cu–N units form linear N–Cu–N ··· N–Cu–N ··· N–Cu–N ··· N–Cu–N ··· chains (*i.e.*, ∠Cu–N ··· N = 180°) where N ··· N refers to the end two nitrogen atoms

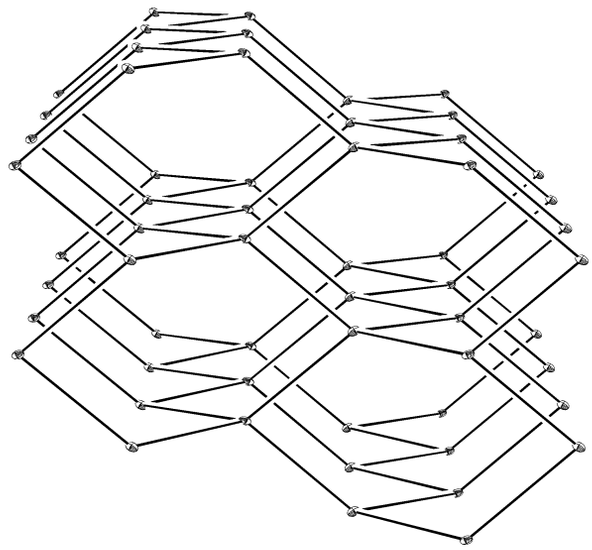

Fig. 6 Connectivity of the Cu^{2+} cations within the framework of **2** illustrating the diamond-like topology. The bipy ligands have been omitted for clarity.

of the spacer ligands pyz or bipy. These linear chains are further connected by the O–Cu–O ··· O–Cu–O ··· O–Cu–O ··· O–Cu–O ··· linkages, where O ··· O represents the oxygen atoms of $(HCO_2)^-$. It is noted that the Cu–O ··· O and Cu–O ··· O linkages are strongly bent (*i.e.*, ∠Cu–O(1) ··· O(2) = 128.5° and ∠O(1) ··· O(2)–Cu = 120.5° in **1**, and ∠Cu–O(1) ··· O(2) = 129.7° and ∠O(1) ··· O(2)–Cu = 117.1° in **2**).

4 Magnetic properties

T-dependent behavior

The variable-temperature magnetic behavior of polycrystalline samples of **1** and **2** were measured between 1.6 and 300 K using complimentary ac susceptibility and dc magnetization techniques. The magnetic data for **1** and **2** are shown in Fig. 7 and 8, respectively.

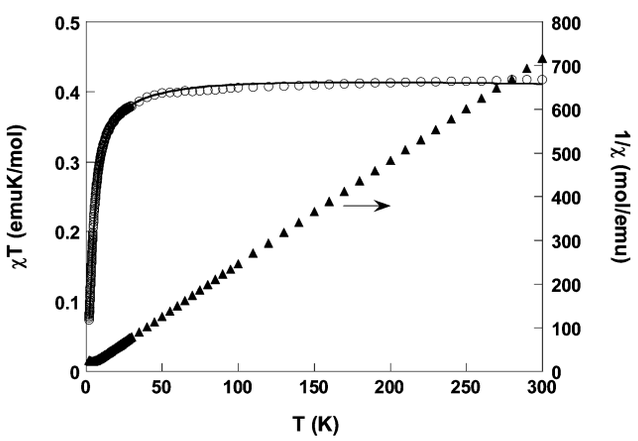

Fig. 7 Plot of χT and $1/\chi$ for $Cu(HCO_2)_2(pyz)$, **1**, collected between 1.6 and 300 K. The solid line is the best fit to the Bonner–Fisher 1D chain model as described in the text.

At ambient temperature, the χT-value for **1** is 0.42 emu K mol^{-1}, which is only slightly larger than the expected value of 0.375 emu K mol^{-1} (for $g = 2$) owing to g-value anisotropy of the Cu^{2+} ion. Upon cooling, $\chi T(T)$ remains fairly constant until ~45 K where it decreases abruptly and continuously down to 1.6 K, where a value of 0.074 emu K mol^{-1} is reached. The rapid decrease in χT is a result of moderate antiferromagnetic exchange interactions between nearest-neighbor $S = 1/2$ Cu^{2+} sites. Subsequently, the $\chi T(T)$ data were fitted to a Curie–Weiss

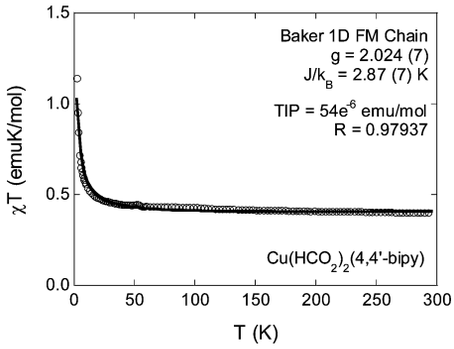

Fig. 8 Plot of χT for $Cu(HCO_2)_2$(bipy), **2**, obtained between 1.6 and 300 K. The solid line is the fit to Baker expression for 1D S = 1/2 ferromagnetic chains.

expression between 10 and 300 K, which yielded $g = 2.12(1)$ and $\theta = -3.24(1)$ K. As an initial test, the $\chi T(T)$ and $\chi(T)$ data were individually fit to the Bonner–Fisher 1D antiferromagnetic chain model.[15] Excellent agreement was obtained in either case, giving $g = 2.14(1)$, $J/k_B = -3.94(1)$ K and TIP = -60×10^{-6} emu mol^{-1}. The expression, eqn. (1), which relates the J-value of a low-dimensional magnetic system to the temperature at which point $\chi(T)$ reaches a maximum, T_{max}, gave a comparable result (−4.14 K) and further supports the 1D formalism for **1**.[16] The exchange constant, J/k_B, is comparable to values observed in other magnetic Cu(II)–pyz systems.[17] Furthermore, a broad maximum in $\chi(T)$ was observed at 3.9 K that signifies short-range and not long-range magnetic ordering. It will be shown in Section 5 that the magnetic behavior is indeed 1D and arises from the Cu–pyz–Cu spin–spin interaction.

$$k_B T_{max}/J = 1.12S(S + 1) + 0.10 \qquad (1)$$

The T-dependent magnetic behavior of **2** differs markedly from that of **1**. At 300 K, χT has a value of 0.40 emu K mol^{-1} and, owing to g-value anisotropy, this value exceeds the expected value of 0.375 emu K mol^{-1} for isotropic and uncoupled spin 1/2 ions. Upon cooling to low temperature, $\chi T(T)$ is nearly flat until ~50 K, increases below ~50 K, and then rapidly increases below ~20 K owing to ferromagnetic correlations (Fig. 8). A final value of 1.87 emu K mol^{-1} is reached at 2 K, at which point, no maximum is observed. A Curie–Weiss analysis of the $1/\chi$ data over the full T-range yields $g = 2.03(1)$ and $\theta = 3.94(1)$ K. To determine the magnitude of the exchange interaction between the Cu ions, the $\chi T(T)$ data were also fitted to the Baker expression for ferromagnetically coupled 1D chains.[18] This yielded satisfactory agreement for $g = 2.02(1)$ and $J/k_B = 2.87(7)$ K.

H-dependent behavior

The field-dependent magnetization, $M(H)$ was acquired at 4.5 K, which is above T_N, for both **1** and **2**, Fig. 9. $M(H)$ rises linearly for **1** up to 7 T which attests to the antiferromagnetic correlations of the system. For the sake of argument, assuming $M(H)$ continuously increases with linear slope, the saturation magnetization, M_{sat}, would occur near 6000 emu Oe mol^{-1} (~90 kOe) based on the g-value obtained from the Curie–Weiss fit. In contrast, **2** shows a nonlinear field-dependent behavior and is continually curving with decreasing slope upon steadily increasing the applied field. A saturation magnetization does not occur over the measured field range, although a value of 5450 emu Oe mol^{-1} is obtained at 7 T that is 95% of the predicted value. The Brillioun magnetization for S = 1/2 and g = 2.025 is shown for comparison in Fig. 9.

5 Discussion

For the simplicity of our discussion, let us choose the local coordinate of the CuO_2N_2 "square" of a distorted CuO_4N_2

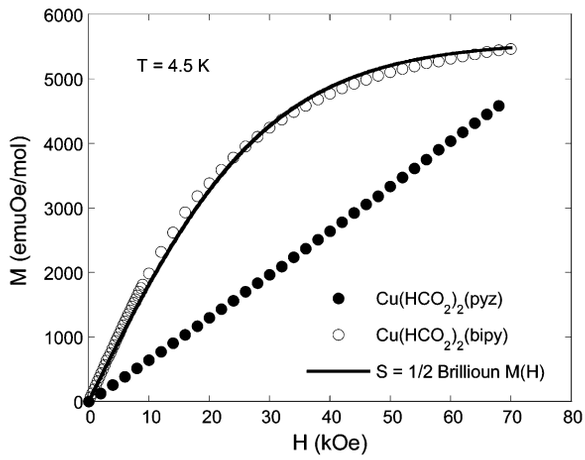

Fig. 9 Isothermal $M(H)$ for **1** and **2** taken at 4.5 K. The Brillioun magnetization calculated at T = 4.5 K for g = 2.025 is shown as a heavy line.

octahedron such that the x- and y-axes run along the Cu–N and Cu–O bonds, respectively. Then the magnetic orbital of each CuO_4N_2 distorted octahedron is given by the $d_{x^2-y^2}$ orbital of Cu that has sigma antibonding contributions of the ligand atom p-orbitals (Fig. 10a).[19,20] The extent of antiferromagnetic interaction through a Cu–L–Cu path, where L refers to a ligand, is strongest when the path is linear.[21] In the previous section it was noted that in both **1** and **2**, the CuO_2N_2 "squares" form linear N–Cu–N ··· N–Cu–N ··· chains and the Cu–O ··· O linkages between these linear chains are strongly bent. In addition, as depicted in Fig. 10b and 10c, the spacer ligand N ··· N (*i.e.*, pyz in **1** and bipy in **2**) has the sigma "lone-pair" orbital that can interact strongly with the $d_{x^2-y^2}$ orbital of Cu. Consequently, it is reasonable to expect that spin exchange interactions are strong only along each linear N–Cu–N ··· N–Cu–N ··· chain in both **1** and **2**. This expectation is consistent with the finding that **1** exhibits 1D antiferromagnetism at low temperatures, but is in contradiction to the observation that **2** exhibits 1D ferromagnetism at low temperatures. To understand the difference between **1** and **2**, we need to carry out a more quantitative analysis to see if the antiferromagnetic interaction in the Cu–N ··· N–Cu path is weak in **2**.

The strengths of spin exchange interactions (*i.e.*, spin exchange parameters J) can be determined on the basis of

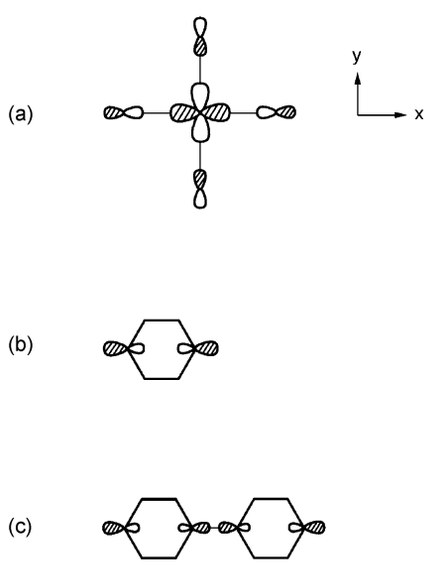

Fig. 10 (a) Schematic representation of the magnetic orbital of a CuO_2N_2 "square". (b) Sigma "lone-pair" orbital of pyz that interacts strongly with the Cu $d_{x^2-y^2}$ orbital. (c) Sigma "lone-pair" orbital of bipy that interacts strongly with the $d_{x^2-y^2}$ orbital of Cu.

first-principles electronic structure calculations in two ways, namely, electronic structure calculations for the high- and low-spin states of spin dimers (*i.e.*, structural units consisting of two spin sites)[22–24] and electronic band structure calculations for various ordered spin arrangements of a magnetic solid.[25] For magnetic solids with large and complex unit cell structures the quantitative methods become difficult to apply. In understanding physical properties of magnetic solids, however, it is sufficient to estimate the relative magnitudes of their J values.[19,20,26–29] In general, a spin exchange parameter J can be written as $J = J_F + J_{AF}$, where the ferromagnetic term J_F (> 0) is small so that the spin exchange becomes ferromagnetic (*i.e.*, $J >$ 0) when the antiferromagnetic term J_{AF} (< 0) is negligibly small in magnitude. Spin exchange interactions of magnetic solids are mostly antiferromagnetic (*i.e.*, $J < 0$), and can be discussed by focusing on the antiferromagnetic terms J_{AF}.[19,20,28,29] When all the spin sites of a magnetic solid are equivalent and have one unpaired spin per site, the J_{AF} term of a spin dimer is given by[30]

$$J_{AF} = -(\Delta e)^2/U_{eff} \quad (2)$$

where Δe is the spin orbital interaction energy, *i.e.*, the energy separation between the two singly occupied orbitals of a spin dimer (Fig. 11) and U_{eff} is the effective on-site repulsion. For a set of closely related magnetic solids, the U_{eff} value should be nearly constant.[19,20,26–29] Trends in the antiferromagnetic spin exchange parameters J values (*i.e.*, $J < 0$) of various magnetic solids are well reproduced by the $-(\Delta e)^2$ values calculated for their spin dimers on the basis of extended Hückel tight binding (EHTB) electronic structure calculations.[19,20,28,29] In these calculations, it is found necessary to employ double-ζ Slater type orbitals (DZ STOs)[31] for both the 3d orbitals of the transition metal and the σ/π orbitals of the surrounding ligand atoms.

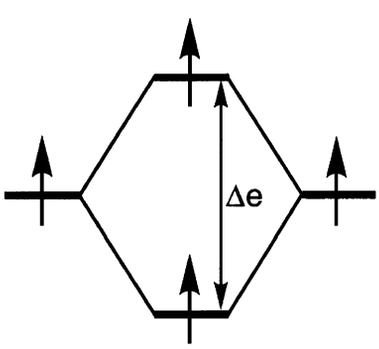

Fig. 11 Orbital interaction diagram between two magnetic sites in a spin dimer, where the spin orbital interaction energy, Δe, is defined as the energy difference of the two singly filled orbitals of the spin dimer.

We now evaluate the relative strengths of the various spin exchange interactions of **1** and **2** by calculating the Δe values for their spin dimers. In **1** and **2** each Cu^{2+} ion is surrounded by four $(HCO_2)^-$ anions and two neutral ligands L (*i.e.*, pyz in **1** and bipy in **2**). Thus the L-bridged spin dimer is given by the $[Cu_2(HCO_2)_8(L)_3]^{4-}$ cluster anion, and the $(HCO_2)^-$-bridged spin dimer by the $[Cu_2(HCO_2)_7(L)_4]^{3-}$ cluster anion. The atomic orbital parameters of Cu, C, N, O and H employed for our extended Hückel tight-binding calculations are listed in the ESI (Table S1).† Our calculations show that the Δe values are practically zero for the $(HCO_2)^-$-bridged spin dimers, but are large for the L-bridged spin dimers [*i.e.*, 570 meV for L = pyz, and 420 meV for L = bipy]. One should not infer from this finding that spin exchange interactions through a HCO_2 bridge are always weak. For example, consider $Cu(HCO_2)_2(H_2O)_2{\cdot}2H_2O$ in which each Cu^{2+} site has four short Cu–O bonds with HCO_2 ligands and two long Cu–O bonds with H_2O, and each Cu^{2+} site is bridged to four neighboring Cu^{2+} sites by HCO_2 to form a layer. Our calculations for $Cu(HCO_2)_2(H_2O)_2{\cdot}2H_2O$ indicate that the spin exchange interaction between adjacent Cu^{2+} sites *via* HCO_2 would be substantially antiferromagnetic (*i.e.*, Δe = 186 meV). Specifically, the magnitude of a spin exchange interaction *via* a certain bridging ligand depends on the nature of the ligand as well as on the geometrical arrangement of the ligand.

According to the Δe values and eqn. (2), the antiferromagnetic spin exchange interaction is stronger in **1** than in **2** by a factor of 2. This is important because it clearly indicates that the antiferromagnetic interaction in the Cu–N ··· N–Cu path of **2** is not negligible. At this stage it is necessary to speculate why **2** shows ferromagnetic behavior at low temperatures. In order to induce ferromagnetic coupling between adjacent Cu^{2+} sites along the linear N–Cu–N ··· N–Cu–N ··· chain, it is necessary to cut off the antiferromagnetic interaction in the Cu–N ··· N–Cu path. The latter can be achieved if **2** undergoes a structural phase transition at a low temperature such that the Cu–O bonds become shorter while the Cu–N bonds become longer in each CuO_4N_2 distorted octahedron. If such a switch of the Jahn–Teller axes occurs, the plane of the magnetic orbital would lie in the CuO_4 "square" so that the antiferromagnetic interaction in the Cu–N ··· N–Cu path would vanish. Work is in progress to test this possibility.

6 Concluding remarks

The formate anion, HCO_2^-, is a suitable ligand to assemble various molecular architectures. However in the two examples described in this paper, the anion does not significantly contribute to the magnetic behavior as demonstrated by electronic structure calculations. It is interesting to point out that 2D magnetism is presented by the parent $Cu(HCO_2)_2(H_2O)_2{\cdot}2H_2O$ compound but not by **1** or **2**, which exemplifies the spin directionality imparted by the organic pyz and 4,4′-bipy moities. We are extending this work to include the other first row transition metals in addition to other organic spacer ligands. Additionally, the microscopic aspects of the magnetic behavior are being investigated using polarized neutron diffraction and inelastic neutron scattering methods.

Acknowledgements

Work performed at Argonne National Laboratory and North Carolina State University was supported by the Office of Basic Energy Sciences, Division of Materials Science, U.S. Department of Energy under contract W-31-109-ENG-38 and grant No. DE-FG02-86ER45259, respectively. Oak Ridge National Laboratory is managed by UT-Battelle, LLC for the U.S. Department of Energy under contract no. DE-AC05-00OR22725.

References

1 (*a*) S. Ferlay, T. Mallah, R. Ouahes, P. Veillet and M. Verdaguer, *Nature*, 1995, **378**, 701; (*b*) J. Larionova, J. Sanchiz, S. Gohlen, L. Ouahab and O. Kahn, *Chem. Commun.*, 1998, 953; (*c*) V. Gadet, T. Mallah, I. Castro and M. Verdaguer, *J. Am. Chem. Soc.*, 1992, **114**, 9213; (*d*) T. Mallah, S. Ferlay, C. Auberger, C. Helary, F. L'Hermite, F. Ouahes, J. Vaissermann, M. Verdaguer and P. Veillet, *Mol. Cryst. Liq. Cryst.*, 1995, **273**, 141; (*e*) W. R. Entley and G. S. Girolami, *Science*, 1995, **268**, 397; (*f*) S. M. Holmes and G. S. Girolami, *J. Am. Chem. Soc.*, 1999, **121**, 5593; (*g*) O. Hatlevik, W. E. Buschmann, J. Zhang, J. L. Manson and J. S. Miller, *Adv. Mater.*, 1999, **11**, 914.

2 (*a*) J. L. Manson, A. M. Arif and J. S. Miller, *Chem. Commun.*, 1999, 1479; (*b*) H.-Y. Shen, W.-M. Bu, E.-Q. Gao, D.-Z. Liao, Z.-H. Jiang, S.-P. Yan and G.-L. Wang, *Inorg. Chem.*, 2000, **39**, 396; (*c*) F. A. Mautner, R. Cortés, L. Lezama and T. Rojo, *Angew. Chem., Int. Ed. Engl.*, 1996, **35**, 78; (*d*) A. K. Gregson and N. T. Moxon, *Inorg. Chem.*, 1982, **21**, 586; (*e*) A. Escuer, R. Vicente, M. A. S. Goher and F. A. Mautner, *Inorg. Chem.*, 1996, **35**, 6386; (*f*) A. Escuer, R. Vicente, M. A. S. Goher and F. A. Mautner,

Inorg. Chem., 1998, **37**, 782; (*g*) L. K. Thompson, S. S. Tandon, F. Lloret, J. Cano and M. Julve, *Inorg. Chem.*, 1997, **36**, 3301; (*h*) R. Cortés, L. Lezama, J. L. Pizarro, M. I. Arriortua and T. Rojo, *Angew. Chem., Int. Ed. Engl.*, 1996, **35**, 1810; (*i*) S. Han, J. L. Manson, J. K. Kim and J. S. Miller, *Inorg. Chem.*, 2000, **39**, 4182.

3 *E.g.* (*a*) H. Tamaki, Z. J. Zhong, N. Matsumoto, S. Kida, K. Koikawa, N. Achiwa and H. Okawa, *J. Am. Chem. Soc.*, 1992, **114**, 6974; (*b*) C. Mathoniere, C. J. Nuttall, S. G. Carling and P. Day, *Inorg. Chem.*, 1996, **35**, 1201; (*c*) S. Decurtins, H. W. Schmalle, P. Schneuwly, J. Ensling and P. Gütlich, *J. Am. Chem. Soc.*, 1994, **116**, 9521.

4 (*a*) C. Oldham, *Prog. Inorg. Chem.*, 1968, **10**, 223; (*b*) R. J. Doedens, *Prog. Inorg. Chem.*, 1976, **21**, 209.

5 B. N. Figgis and R. L. Martin, *J. Chem. Soc. A*, 1956, 3837; B. N. Figgis and R. L. Martin, *J. Chem. Soc. A*, 1957, 2545.

6 (*a*) R. B. Flippen and S. A. Friedberg, *J. Chem. Phys.*, 1963, **38**, 2652; (*b*) H. Abe, *Phys. Rev.*, 1953, **92**, 1572; (*c*) J. Shimada, H. Abe and K. Ono, *J. Phys. Soc. Jpn.*, 1956, **11**, 137; (*d*) G. R. Wagner and S. A. Friedberg, *Phys. Lett.*, 1964, **9**, 11.

7 (*a*) H. M. Rønnow, D. F. McMorrow and A. Harrison, *Phys. Rev. Lett.*, 1999, **82**, 3152; (*b*) S. J. Clarke, A. Harrison, T. E. Mason, G. J. McIntyre and D. Visser, *J. Phys.: Condens. Matter*, 1992, **4**, L71.

8 (*a*) R. Kiriyama, H. Ibamoto and K. Matsuo, *Acta Crystallogr.*, 1954, **7**, 482; (*b*) T. R. Lomer, *Acta Crystallogr., Sect. B*, 1971, **27**, 859; (*c*) K. Okada, M. I. Kay, D. T. Cromer and I. Almodovar, *J. Chem. Phys.*, 1966, **44**, 1648.

9 A. J. Schultz, D. G. Van Derveer, D. W. Parker and J. E. Baldwin, *Acta Crystallogr., Sect. C*, 1990, **46**, 276.

10 A. J. Schultz, *Trans. Am. Crystallogr. Assoc.*, 1987, **23**, 283.

11 R. A. Jacobson, *J. Appl. Crystallogr.*, 1986, **19**, 283.

12 G. M. Sheldrick, SHELXL-97, Program for refinement of crystal structures, University of Göttingen, Germany, 1997; G. M. Sheldrick, SHELXTL, Structure Determination Programs, Version 5.1, Bruker Analytical X-ray Systems, Madison, WI, USA, 1998.

13 (*a*) J. L. Manson, Q.-z. Huang, J. W. Lynn, H.-J. Koo, M.-H. Whangbo, R. Bateman, T. Otuska, N. Wada, D. N. Argyriou and J. S. Miller, *J. Am. Chem. Soc.*, 2001, **123**, 162; (*b*) J. L. Manson, C. D. Incarvito, A. L. Rheingold and J. S. Miller, *J. Chem. Soc., Dalton Trans.*, 1998, 3705.

14 S. J. Rettig, R. C. Thompson, J. Trotter and S. Xia, *Inorg. Chem.*, 1999, **38**, 1360.

15 J. C. Bonner and M. E. Fisher, *Phys. Rev. A*, 1964, **135**, 640.

16 M. E. Lines, *J. Phys. Chem. Solids*, 1970, **31**, 101.

17 (*a*) J. Darriet, M. S. Haddad, E. N. Duesler and D. N. Hendrickson, *Inorg. Chem.*, 1979, **18**, 2679; (*b*) H. W. Richardson and W. E. Hatfield, *J. Am. Chem. Soc.*, 1976, **98**, 835; (*c*) P. Jensen, S. R. Batten, G. D. Fallon, D. C. R. Hockless, B. Moubaraki, K. S. Murray and R. Robson, *J. Solid State Chem.*, 1999, **145**, 387; (*d*) J. S. Haynes, S. J. Rettig, J. R. Sams, R. C. Thompson and J. Trotter, *Can. J. Chem.*, 1987, **65**, 420.

18 G. A. Baker, G. S. Rushbrooke and H. E. Gilbert, *Phys. Rev. A*, 1964, **135**, 1272.

19 M.-H. Whangbo and H.-J. Koo, *Inorg. Chem.*, 2001, **40**, 2169.

20 M.-H. Whangbo and H.-J. Koo, *Inorg. Chem.*, 2002, **41**, 3570.

21 J. B. Goodenough, *Magnetism and the Chemical Bond*, Wiley, Cambridge, MA, 1963.

22 F. Illas, I. de P. R. Moreira, C. de Graaf and V. Barone, *Theor. Chem. Acc.*, 2000, **104**, 265 and the references cited therein.

23 L. Noodleman, *J. Chem. Phys.*, 1981, **74**, 5737.

24 D. Dai and M.-H. Whangbo, *J. Chem. Phys.*, 2001, **114**, 2887; D. Dai and M.-H. Whangbo, *J. Chem. Phys.*, 2003, **118**, 29.

25 S. E. Derenzo, M. K. Klitenberg and M. J. Weber, *J. Chem. Phys.*, 2000, **112**, 2074 and the references cited therein.

26 O. Kahn, *Molecular Magnetism*, VCH Publishers, Weinheim, 1993.

27 P. J. Hay, J. C. Thibeault and R. Hoffmann, *J. Am. Chem. Soc.*, 1975, **97**, 4884.

28 H.-J. Koo, M.-H. Whangbo, P. D. VerNooy, C. C. Torardi and W. J. Marshall, *Inorg. Chem.*, 2002, **41**, 4664 and the references cited therein.

29 M.-H. Whangbo, H.-J. Koo and D. Dai, *J. Solid State Chem.*, in press.

30 This expression is valid when spin exchange parameters of a spin Hamiltonian are written as J instead of $2J$.

31 E. Clementi and C. Roetti, *At. Data Nucl. Data Tables*, 1974, **14**, 177.